JOURNAL OF Materials CHEMISTRY

Preparation of $Y_2O_3:Eu^{3+}$ phosphor fine particles using an emulsion liquid membrane system

Takayuki Hirai,*[a] Takashi Hirano[a] and Isao Komasawa[a,b]

[a]*Department of Chemical Science and Engineering, Graduate School of Engineering Science, Osaka University, Toyonaka 560-8531, Japan. E-mail: hirai@cheng.es.osaka-u.ac.jp*
[b]*Research Center for Photoenergetics of Organic Materials, Osaka University, Toyonaka 560-8531, Japan*

Received 30th March 2000, Accepted 31st May 2000
First published as an Advanced Article on the web 6th September 2000

$Y_2O_3:Eu^{3+}$ phosphor particles were obtained by calcination of composite Y–Eu oxalate particles prepared in emulsion liquid membrane (ELM, water-in-oil-in-water (W/O/W) emulsion) systems. In the ELM systems, composite Y–Eu particles could be prepared by transporting either Y^{3+} and Eu^{3+} ions or oxalate ions from the external water phase into the internal water phase, employing proper ELM systems, where bis(1,1,3,3-tetramethylbutyl)phosphinic acid (DTMBPA) or 2-methyl-2-ethylheptanoic acid (VA-10) was used as an extractant (cation carrier), or tri-*n*-octylamine (TNOA) was used as an anion carrier. These ELM systems were effective for preparing size (submicrometer) and morphology (spherical) controlled composite Y–Eu oxalate particles in the internal water droplets. The $Y_2O_3:Eu^{3+}$ particles obtained by calcination of the composite oxalate particles showed photoluminescence at 614 nm.

Introduction

An emulsion liquid membrane (ELM, water-in-oil-in-water (W/O/W) emulsion) system has been studied for the selective separation of metals, in which the metal ions in the external water phase are extracted into the organic membrane phase, and then stripped and concentrated into the internal water phase. Recently, it has been found that the internal water phase is capable of being used for the preparation of size-controlled and morphology-controlled fine particles, since the micrometer-sized internal water droplet has a restricted reaction area. The internal water droplet is also remarkable in respect to its rather hydrophobic property compared to homogeneous aqueous solutions, which allows the formation of particles of lower hydration number and thus characteristic morphology. In addition, since the ELM system has a high selectivity, purification and pre-concentration of the target metals are not needed. The preparation of single-component fine particles, such as rare-earth oxalate particles,[1–3] using the ELM system, has been investigated. The method is also applicable for the preparation of composite particles: the preparation of composite Sr–Pb oxalate particles[4] and acicular ferrite particles[5] using the ELM system, where two different metal ions are transported into the internal phase, has also been reported.

$Y_2O_3:Eu^{3+}$, which is available commercially, is known to be one of the most promising red phosphors for field emission display applications.[6] Phosphor particles which have spherical morphology, submicrometer sizes, and narrow particle size distribution give higher packing densities than commercial products (3–5 μm in size), and are thus effective in enhancement of luminescent efficiency.[6–9] In previous studies,[2,3] Y oxalate particles of submicrometer size were prepared in the ELM system containing 2-methyl-2-ethylheptanoic acid (VA-10) and bis(1,1,3,3-tetramethylbutyl)phosphinic acid (DTMBPA) as the extractant (cation carrier). In the VA-10 system, ultrafine particles of 20–60 nm in diameter were obtained, while spherical oxalate particles of 0.2–0.6 μm in diameter were obtained in the DTMBPA system. Thus, when these ELM methods are extended to the preparation of composite oxalate particles containing two or more different rare earth metals, the morphology and composition of the particles are expected to be controllable by controlling the transport (extraction and stripping) of the metals. In the present work, therefore, composite Y–Eu oxalate fine particles are prepared in the ELM systems, by feeding Eu ions into the external water phase together with Y ions. In this, ELM systems containing DTMBPA or VA-10 as cation carrier are employed. It is also possible to prepare oxalate particles by feeding oxalate anions into the external phase and transporting to the internal water phase in which Eu and Y ions are contained. In this case, the ELM system containing tri-*n*-octylamine (TNOA) is employed as the anion carrier. The oxalate particles thus obtained are calcined to oxide, $Y_2O_3:Eu^{3+}$. The size, morphology, and luminescence properties of the oxide particles are then investigated.

Experimental

Chemicals and procedures

Bis(1,1,3,3-tetramethylbutyl)phosphinic acid (DTMBPA) was supplied by Nippon Chemical Industrial Co. Ltd., Tokyo. Tertiary aliphatic monocarboxylic acid VA-10 (2-methyl-2-ethylheptanoic acid) was supplied by Shell Chemical Co. Tri-*n*-octylamine (TNOA), YCl_3, $EuCl_3$, sodium acetate, ethylene glycol, and oxalic acid were supplied by Wako Pure Chemical Industries, Ltd. Sorbitan sesquioleate (Span 83) was supplied by Tokyo Kasei Kogyo Co. Ltd., Tokyo.

The oxalate particles were prepared *via* a procedure similar to that reported previously for the DTMBPA[3] and VA-10 systems.[2] The organic membrane phase was kerosene containing 5 wt% Span 83 and 0.5 mol l^{-1} DTMBPA or VA-10. This was mixed with the internal water phase (0.1 mol l^{-1} oxalic acid) at a volume ratio of 1 : 1, and emulsified mechanically by use of a homogenizer (12 000 rpm). The mean diameter of the internal water droplets was *ca.* 3 μm.[2,3] The resulting W/O emulsion (10 ml) was poured into the external water phase (50 ml of YCl_3 and $EuCl_3$ aqueous solution) and stirred vigorously by a magnetic stirrer to form a W/O/W emulsion. $[Y^{3+}]+[Eu^{3+}]$ in the feed external solution was kept at

 DOI: 10.1039/b002532l

4 mmol l^{-1}, and the feed molar ratio, $\{[Eu]/([Y]+[Eu])\}_f$, was varied. CH_3COONa (0.02 mol l^{-1}) was added to the external phase for the VA-10 system, to maintain the external phase pH above 4. The size of the W/O emulsion drops dispersed in the external phase was less than 2 mm. After stirring for the required time, the W/O emulsion was separated from the external water phase and demulsified by adding *ca.* 70 ml of ethylene glycol or acetone. The particles, formed in the internal water droplets, were separated by centrifugation and were washed with acetone. When TNOA was used as the anion carrier, the organic membrane phase was prepared by dissolving 5 wt% Span 83 and 0.1 mol l^{-1} TNOA in kerosene. This was emulsified with the internal water phase (YCl_3 and $EuCl_3$ aqueous solution, $[Y^{3+}]+[Eu^{3+}]=0.02$ mol l^{-1}), and the resulting W/O emulsion was dispersed in the external water phase (2 mmol l^{-1} oxalic acid), to make composite oxalate particles. The oxalate particles were calcined in air, in the temperature range of 1073–1423 K for 2 h, to obtain the oxide particles, $Y_2O_3:Eu^{3+}$.

Analyses

The composite oxalate and oxide particles obtained were characterized by means of scanning electron microscopy (SEM, Hitachi S-5000), thermal analysis (TG-DTA, Shimadzu TG-DTA50), and powder X-ray diffraction (XRD, 40 kV and 30 mA, CuK_α, Philips PW-3050). Prior to SEM examination, all the samples were sputter-coated with a *ca.* 10 nm thick platinum layer, in order to minimize any possible surface charging effects. The mean crystallite size was estimated from the full width at half maximum of the diffraction peak by the Sherrer equation:[10,11]

$$D = 0.89\ \lambda/\{\beta(2\theta)\ \cos\theta\} \quad (1)$$

where $\beta(2\theta)$ is the width of the pure diffraction profile in radians, λ is the wavelength of the X-rays (0.154056 nm), θ is the diffraction angle, and D is the average diameter of the crystallite.

To determine the rare earth metal concentrations in the organic membrane phase, the W/O emulsion was demulsified electrically and the organic phase was stripped with 1 mol l^{-1} HCl solution. The metal concentrations in the resulting HCl and the external aqueous solutions were measured using an inductively coupled argon plasma emission spectrometer (ICP-AES, Nippon Jarrell-Ash ICAP-575 MarkII). The metal concentrations in the internal water phase were then calculated by mass balance. The molar ratio of Eu in the particles, $\{[Eu]/([Y]+[Eu])\}_p$, was determined using ICP-AES, following dissolution of the particles in concentrated HCl solution. The concentrations of oxalic acid in the external water phase and the organic membrane phase were determined by potentiometric titration using an automatic titration apparatus (Hiranuma Comtite-550). The oxalic acid concentration in the internal water phase was calculated by mass balance. The measurement of photoluminescence spectra of the particles was carried out with a spectrofluorometer (JASCO FP-777, Xe lamp, excitation wavelength: 254 nm), following dispersion of 1 mg of the particles in 10 ml of ethanol using an ultrasonic bath. A laser scattering particle-size distribution analyzer (Horiba LA-910W) was used to measure the size of the particles.

Results and discussion

Characterization of composite Y–Eu oxalate particles prepared in the ELM systems

The SEM images of composite Y–Eu oxalate particles obtained at $\{[Eu]/([Y]+[Eu])\}_f=0.1$ in DTMBPA, VA-10, and TNOA systems are shown in Fig. 1. Well-defined spherical particles ranging from 60 to 400 nm in diameter are obtained in the DTMBPA system (Fig. 1(a)). The particles prepared in the VA-10 system (Fig. 1(b)) are spherical and about 200 nm in diameter, together with smaller particles of *ca.* 20–30 nm in diameter. Well-defined spherical particles ranging from 60 to 200 nm in diameter are obtained in the TNOA system (Fig. 1(c)). The size and morphology of the composite particles obtained in the DTMBPA and VA-10 systems are similar to those for the Y oxalate particles obtained in the respective ELM systems.[2,3] Composite oxalate particles prepared from a homogeneous aqueous solution, by adding 0.04 mol l^{-1} rare earth chloride solution ($\{[Eu]/([Y]+[Eu])\}_f=0.1$) to 0.1 mol l^{-1} oxalic acid solution, are not spherical but are tabular and elongated, and the particle size was greater than 1 μm, as shown in Fig. 2. The ELM systems are therefore effective in controlling the particle size and morphology. The oxalate particles prepared in the ELM systems showed few characteristic XRD peaks, and therefore are composite Y–Eu oxalate of low crystallinity, while the particles prepared in the homogeneous

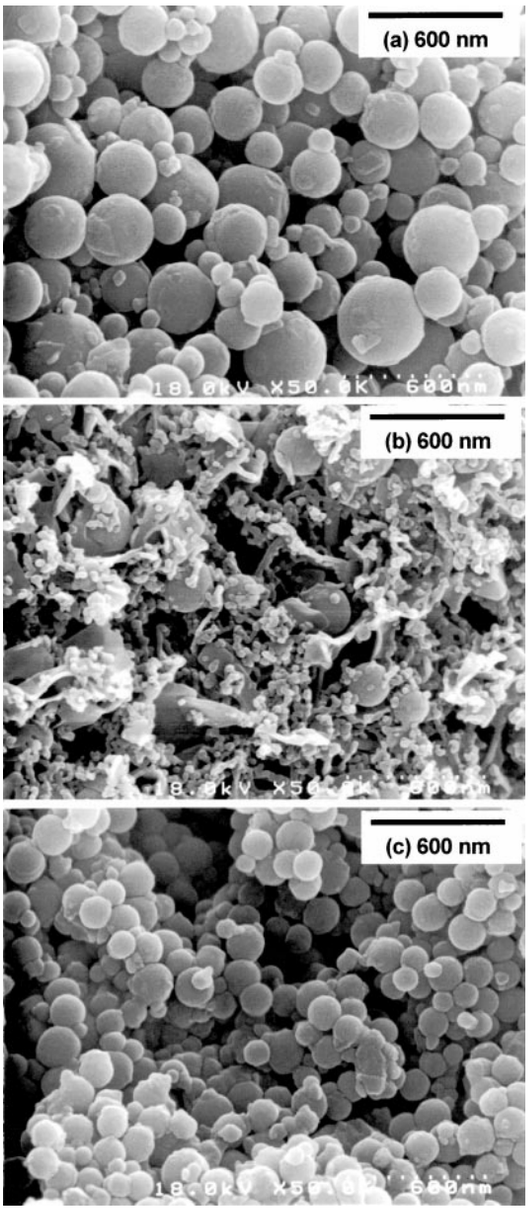

Fig. 1 SEM images for the composite Y–Eu oxalate particles obtained at $\{[Eu]/([Y]+[Eu])\}_f=0.1$ in the (a) DTMBPA, (b) VA-10, and (c) TNOA systems.

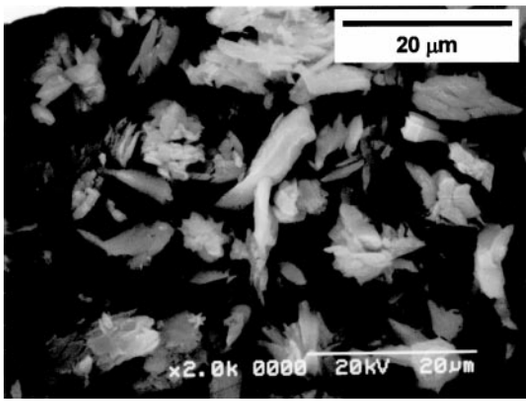

Fig. 2 SEM image for the composite Y–Eu oxalate particles obtained at $\{[Eu]/([Y]+[Eu])\}_f=0.1$ in the homogeneous aqueous solution.

solution showed characteristic diffraction peaks corresponding to rare earth oxalate decahydrate.

Composition of the particles

The time-course variations in the mole fractions for the Y and Eu ions in the external water phase, organic membrane phase, and internal water phase in the DTMBPA and VA-10 systems are shown in Fig. 3. In the DTMBPA system, the extraction proceeds rather slowly, especially for Eu, and only 70% of the Y and Eu ions are transported into the internal water phase during 2 h of stirring. In the VA-10 system, the transport of the Eu ions into the internal phase occurs in preference to the transport of Y, and is completed in 30 min. The final molar ratio of the two metals moved into the internal water phase is almost identical to the feed molar ratio, $\{[Eu]/([Y]+[Eu])\}_f$, in both systems. Fig. 4 shows the time-course variations in the mole fractions for oxalate ion in the TNOA system at $\{[Eu]/([Y]+[Eu])\}_f=0.1$. The transport of the oxalate ion into the internal water phase is completed in 10 min, while about 10% of oxalate ion is retained in the organic phase and external water phase.

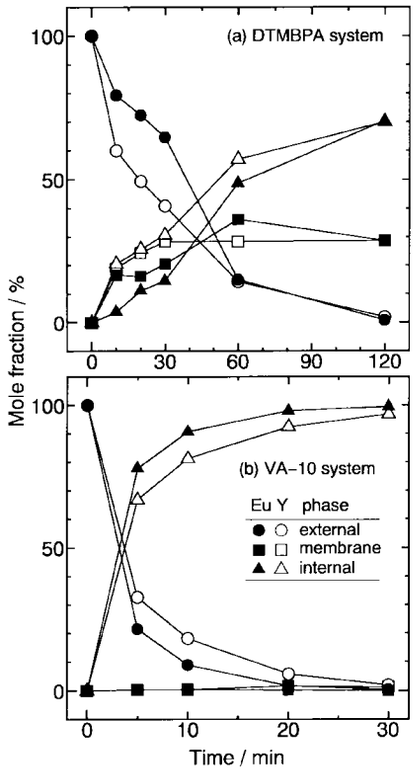

Fig. 3 Time-course variation for the mole fractions of Y and Eu in the external water phase, organic membrane phase, and internal water phase in the (a) DTMBPA and (b) VA-10 systems at $\{[Eu]/([Y]+[Eu])\}_f=0.1$. The mole fraction in the initial external water phase is set as 100%.

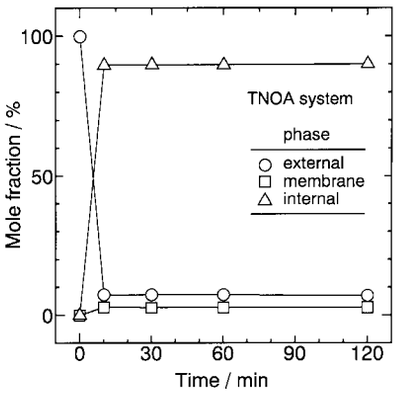

Fig. 4 Time-course variation for the mole fractions of oxalic acid in the external water phase, organic membrane phase, and internal water phase in the TNOA system at $\{[Eu]/([Y]+[Eu])\}_f=0.1$. The mole fraction in the initial external water phase is set as 100%.

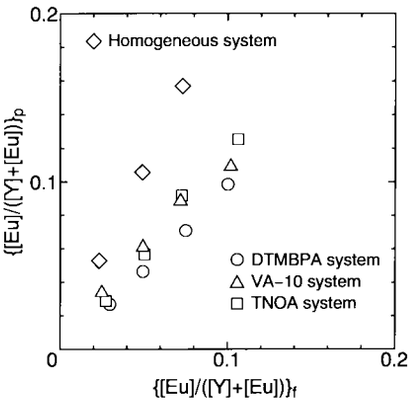

Fig. 5 Relationship between the feed molar ratio, $\{[Eu]/([Y]+[Eu])\}_f$, and the composition of the particles, $\{[Eu]/([Y]+[Eu])\}_p$ for the particles prepared in a homogeneous system, by mixing 0.1 mol l^{-1} YCl_3+EuCl_3 aqueous solution with 0.1 mol l^{-1} oxalic acid solution at a volume ratio of 2 : 1, and in the ELM systems.

Fig. 5 shows the particle composition of the particles, $\{[Eu]/([Y]+[Eu])\}_p$. When the composite oxalate particles were prepared in a homogeneous system, by mixing 0.1 mol l^{-1} YCl_3+EuCl_3 aqueous solution with 0.1 mol l^{-1} oxalic acid solution at a volume ratio of 2 : 1, it was found that Eu oxalate precipitated preferentially to Y oxalate. This difference in the precipitation rate may be a main cause of the result that $\{[Eu]/([Y]+[Eu])\}_p > \{[Eu]/([Y]+[Eu])\}_f$ for the particles prepared in the VA-10 and TNOA systems. In the DTMBPA system, $\{[Eu]/([Y]+[Eu])\}_p$ is almost identical to $\{[Eu]/([Y]+[Eu])\}_f$. The difference in the precipitation rate (Eu > Y) may be cancelled in this case, since the transport of Y is faster than Eu when DTMBPA is employed as the cation carrier.

Calcination of the oxalate particles

Calcination of the composite Y–Eu oxalate particles, prepared in the ELM and homogeneous systems at $\{[Eu]/([Y]+[Eu])\}_f=0.1$, was performed to obtain $Y_2O_3:Eu^{3+}$ particles. Fig. 6 shows the TG-DTA curve for the oxalate particles prepared in the DTMBPA system, which resembles that obtained for the particles obtained in the homogeneous system. The TG curve indicates weight losses in the temperature ranges from 293 to 473 K and from 573 to 973 K. These weight loss steps are accompanied by an

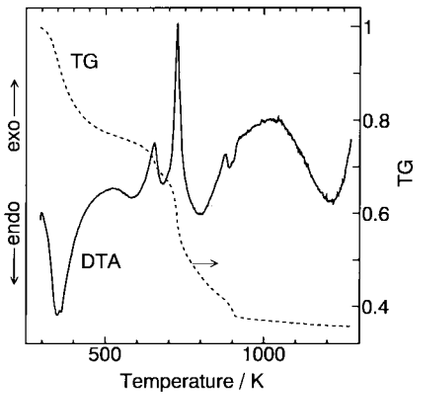

Fig. 6 TG-DTA curve for composite Y–Eu oxalate particles prepared in the DTMBPA system at $\{[Eu]/([Y]+[Eu])\}_f=0.1$.

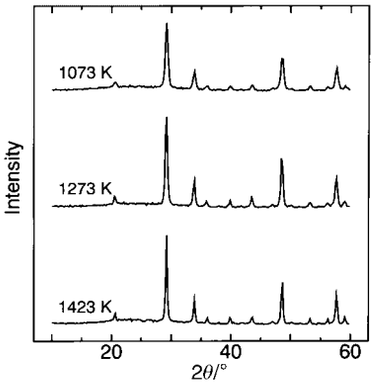

Fig. 7 Effect of calcination temperature on X-ray diffraction patterns for $Y_2O_3:Eu^{3+}$ particles obtained by calcination of composite Y–Eu oxalate particles prepared in the DTMBPA system at $\{[Eu]/([Y]+[Eu])\}_f=0.1$.

endothermic peak (at 363 K) and an exothermic peak (at 723 K) in the DTA curve. They correspond to the conversion of hydrated into anhydrous material, and then into oxide, respectively. These results indicate that calcination above 973 K brings complete decomposition of the oxalate to oxide. The particles prepared in the DTMBPA system calcined at 1073, 1273, and 1423 K were characterized by XRD, as shown in Fig. 7. Calcination of the particles above 1073 K produces the characteristic patterns of Y_2O_3, corresponding to the results of TG-DTA analysis. Similar characteristic XRD patterns of Y_2O_3 were obtained for the particles prepared in the VA-10, TNOA, and homogeneous systems. From the XRD peaks obtained, the crystallite size D of the particles was estimated.

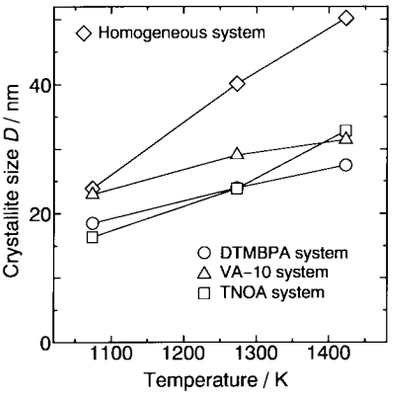

Fig. 8 Effect of the calcination temperature on the crystallite size D for $Y_2O_3:Eu^{3+}$ particles obtained by calcination of composite Y–Eu oxalate particles prepared in the ELM and homogeneous systems at $\{[Eu]/([Y]+[Eu])\}_f=0.1$.

The crystallite size increases with increasing calcination temperature, as shown in Fig. 8, especially for the particles prepared in the homogeneous system. The SEM images for the oxide particles prepared in the ELM systems and calcined at 1273 K are shown in Fig. 9. The calcination of oxalate particles prepared in the DTMBPA and TNOA systems brings about some contraction of the particles, probably caused by H_2O and CO_2 elimination. Oxide particles of smaller than 100 nm are obtained by calcination of the particles prepared in the VA-10 system at 1073 K, and then some sintering of the particles was observed at 1273 K. Sintering of the particles became obvious when these were calcined above 1423 K.

Luminescent properties of the oxide particles

Typical photoluminescence spectra from $Y_2O_3:Eu^{3+}$ particles, prepared in the ELM and homogeneous systems at $\{[Eu]/([Y]+[Eu])\}_f=0.1$ and calcined at 1273 K, are shown in Fig. 10. The main emission peak at 614 nm was observed, which corresponds to a red emission. Sharma *et al.*[9] reported that the emission intensity was increased by reducing the

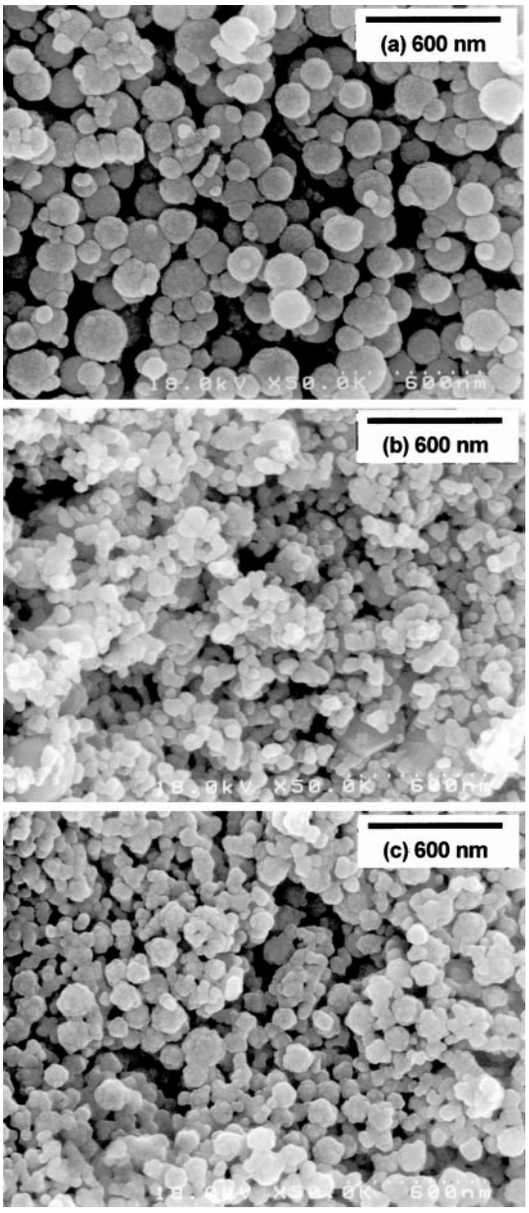

Fig. 9 SEM images for $Y_2O_3:Eu^{3+}$ particles obtained by calcination of composite Y–Eu oxalate particles prepared in the (a) DTMBPA, (b) VA-10, and (c) TNOA systems at $\{[Eu]/([Y]+[Eu])\}_f=0.1$. Calcination temperature: 1273 K.

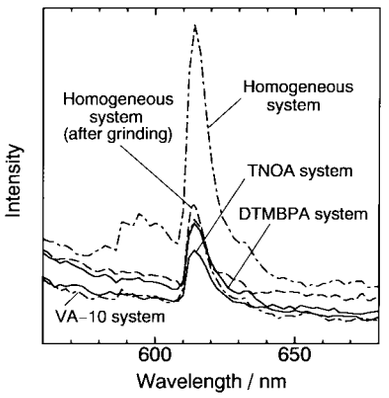

Fig. 10 Photoluminescence spectra from $Y_2O_3:Eu^{3+}$ particles obtained by calcination of composite Y–Eu oxalate particles prepared in the ELM and homogeneous systems. Calcination temperature: 1273 K.

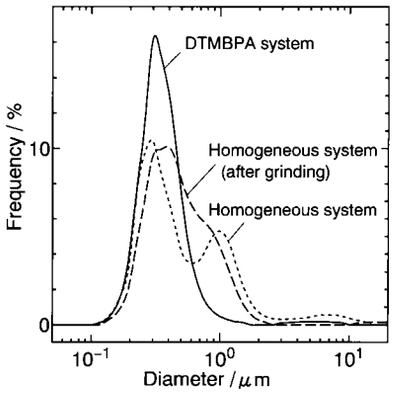

Fig. 11 Size distribution for $Y_2O_3:Eu^{3+}$ particles obtained by calcination of composite Y–Eu oxalate particles prepared in the DTMBPA and homogeneous systems. Calcination temperature: 1273 K.

$Y_2O_3:Eu^{3+}$ particle size from 6 μm to 10 nm. In the present study, on the contrary, the smaller particles prepared in the ELM systems showed lower emission intensities than the larger particles prepared in the homogeneous system, probably due to the smaller crystallite size of the smaller particles (Fig. 8). As shown in Fig. 11, the particles prepared in the homogeneous system have a wider particle size distribution, and therefore the particles were ground in a mortar, to narrow the size distribution, although grinding may cause lattice defects and may decrease emission intensity. The emission intensity from the ground particles was much decreased compared with the original particles, and was comparable to that from the particles prepared in the DTMBPA and VA-10 systems. The greater emission intensity from the particles prepared in the homogeneous system is therefore attributable mainly to particles larger than *ca.* 1 μm. Although it seems to be difficult to prepare particles larger than 1 μm in the ELM system, smaller particles having spherical morphology and narrow size

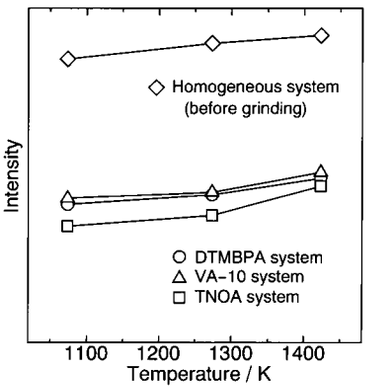

Fig. 12 Effect of calcination temperature on the luminescent intensity from $Y_2O_3:Eu^{3+}$ particles obtained by calcination of composite Y–Eu oxalate particles prepared in the ELM and homogeneous systems at $\{[Eu]/([Y]+[Eu])\}_f=0.1$.

distribution allow a dense coating on substrates such as glass sheets.

Fig. 12 shows the effect of calcination temperature on the luminescent intensity. The greatest intensity was obtained at high calcination temperatures up to 1423 K. Calcination at temperatures higher than 1423 K, however, caused a decrease in the emission intensity, due to the sintering of the particles.

Acknowledgements

The authors are grateful to Mr. Masao Kawashima of the "Gas-Hydrate Analyzing System (GHAS)" of Osaka University for his experimental assistance in characterization of the particles, and to the Division of Chemical Engineering for the Lend-Lease Laboratory System. The authors are also grateful for the financial support through a Grant-in-Aid for Scientific Research (No. 11650781) from the Ministry of Education, Science, Sports and Culture, Japan.

References

1 T. Hirai, N. Okamoto and I. Komasawa, *AIChE J.*, 1998, **44**, 197.
2 T. Hirai, N. Okamoto and I. Komasawa, *J. Chem. Eng. Jpn.*, 1998, **31**, 474.
3 T. Hirai, N. Okamoto and I. Komasawa, *Langmuir*, 1998, **14**, 6648.
4 T. Hirai, J. Kobayashi and I. Komasawa, *J. Chem. Eng. Jpn.*, 1998, **31**, 787.
5 T. Hirai, J. Kobayashi and I. Komasawa, *Langmuir*, 1999, **15**, 6291.
6 S. H. Cho, J. S. Yoo and J. D. Lee, *J. Electrochem. Soc.*, 1998, **145**, 1017.
7 T. G. Ireland, J. Silver, C. Gibbons and A. Vecht, *Electrochem. Solid-State Lett.*, 1999, **2**, 52.
8 Y. C. Kang, S. B. Park, I. W. Lenggoro and K. Okuyama, *J. Phys. Chem. Solids*, 1999, **60**, 379.
9 P. K. Sharma, M. H. Jilavi, R. Nass and H. Schmidt, *J. Lumin.*, 1999, **82**, 187.
10 T. Yoshida, T. Tanaka, H. Yoshida, T. Funabiki, S. Yoshida and T. Murata, *J. Phys. Chem.*, 1995, **99**, 10890.
11 Q. Li, L. Gao and D. Yan, *Nanostruct. Mater.*, 1997, **8**, 825.